Accepted Manuscript




# Knee medial and lateral contact forces in a musculoskeletal model with subject-specific contact point trajectories

A. Zeighami, R. Aissaoui, R. Dumas

PII: S0021-9290(18)30042-3
DOI: https://doi.org/10.1016/j.jbiomech.2018.01.021
Reference: BM 8537

To appear in: *Journal of Biomechanics*

Accepted Date: 14 January 2018

Please cite this article as: A. Zeighami, R. Aissaoui, R. Dumas, Knee medial and lateral contact forces in a musculoskeletal model with subject-specific contact point trajectories, *Journal of Biomechanics* (2018), doi: https://doi.org/10.1016/j.jbiomech.2018.01.021

This is a PDF file of an unedited manuscript that has been accepted for publication. As a service to our customers we are providing this early version of the manuscript. The manuscript will undergo copyediting, typesetting, and review of the resulting proof before it is published in its final form. Please note that during the production process errors may be discovered which could affect the content, and all legal disclaimers that apply to the journal pertain.

ACCEPTED MANUSCRIPT

**Knee medial and lateral contact forces in a musculoskeletal model with subject-specific contact point trajectories**

A. Zeighami[1*], R. Aissaoui[1], R. Dumas[2]

1. Laboratoire de Recherche en Imagerie et Orthopédie (LIO), École de Technologie Supérieure (ÉTS), Centre de Recherche du CHUM, Montréal, Québec, Canada
2. Université Lyon, Université Claude Bernard Lyon 1, IFSTTAR, UMR_T9406, LBMC, F69622, Lyon, France

Ali Zeighami*: zeighamiali87@gmail.com, ali.zeighami.1@ens.etsmtl.ca

Address: Imaging and Orthopaedics Research Laboratory (LIO), École de Technologie Supérieure
The CHUM Research Centre, Viger tower, 900 St-Denis, Room R11.322, Montréal, (QC) H2X0A9, Canada
Tel: +1 (514) 890-8000, ext. 30964
Raphaël Dumas: raphael.dumas@ifsttar.fr

Rachid Aissaoui: rachid.Aissaoui@etsmtl.ca

Type of manuscript: original article.

Running title: A musculoskeletal model with subject-specific contact point trajectories

Word count: 3599.

**Abstract**

Contact point (CP) trajectory is a crucial parameter in estimating medial/lateral tibio-femoral contact forces from the musculoskeletal (MSK) models. The objective of the present study was to develop a method to incorporate the subject-specific CP trajectories into the MSK model. Ten healthy subjects performed 45 second treadmill gait trials. The subject-specific CP trajectories were constructed on the tibia and femur as a function of extension-flexion using low-dose bi-plane x-ray images during a quasi-static squat. At each extension-flexion position, the tibia and femur CPs were superimposed in the three directions on the medial side, and in the anterior-posterior and proximal-distal directions on the lateral side to form the five kinematic constraints of the knee joint. The Lagrange



ACCEPTED MANUSCRIPT

ACCEPTED MANUSCRIPT

multipliers associated to these constraints directly yielded the medial/lateral contact forces. The results from the personalized CP trajectory model were compared against the linear CP trajectory and sphere-on-plane CP trajectory models which were adapted from the commonly used MSK models. Changing the CP trajectory had a remarkable impact on the knee kinematics and changed the medial and lateral contact forces by 1.03 BW and 0.65 BW respectively, in certain subjects. The direction and magnitude of the medial/lateral contact force were highly variable among the subjects and the medial-lateral shift of the CPs alone could not determine the increase/decrease pattern of the contact forces. The suggested kinematic constraints are adaptable to the CP trajectories derived from a variety of joint models and those experimentally measured from the 3D imaging techniques.

Keywords: knee contact force, musculoskeletal model, subject-specific, contact point trajectory, gait.

## Introduction

Current musculoskeletal (MSK) models of the lower limb demonstrated good accuracy in the estimation of the contact forces between femoral and tibial instrumented prosthetic components (Gerus et al., 2013; Jung et al., 2016; Kia et al., 2014; Marra et al., 2015). However, the accuracy of the medial/lateral contact force estimation considerably improved by customizing the point of contact force application (Lerner et al., 2015). The estimation of intact knee joint contact forces still remains a challenge, because the medial and lateral contact forces cannot be well calculated without a good estimate of the subject's contact point (CP) trajectories (Saliba et al., 2017). Such information is very difficult to obtain *in vivo* because it relies on both joint kinematics and articular surface geometries.



ACCEPTED MANUSCRIPT

ACCEPTED MANUSCRIPT

However, recent methods could estimate knee contact parameters in weight-bearing conditions using either bi-plane fluoroscopy (Farrokhi et al., 2016; Farrokhi et al., 2014), or bi-plane low-dose radiography (Zeighami et al., 2017). Biplane imaging allows for a relatively small registration error and yields an estimation of CPs based on the concept of minimal bone-to-bone distance (Zeighami et al., 2017). The CP trajectory predictions were similar to *in vitro* measurements of the center of pressure (Draganich et al., 1987). Each of these studies showed that the trajectory of the center of bone-to-bone proximity reveals inter-subject differences as well as distinctions between healthy and osteoarthritic knees.

Within inverse dynamics computational frameworks, subject-specific joint kinematics has been introduced in MSK models at the step of inverse kinematics (Gerus et al., 2013; Scheys et al., 2011; Valente et al., 2015; Zheng et al., 2014). Nevertheless, the definition of CP trajectories, at the step of joint contact force computation, remains most of the time very basic, i.e. at a fixed distance from the tibial plateau centreline. This fixed distance is typically set at 25% of tibial plateau width (Johnson et al., 1981) in a range from 20 mm (Gerus et al., 2013; Schipplein and Andriacchi, 1991) to 25 mm (Crowninshield, 1978; Lloyd and Buchanan, 1996; Morrison, 1970) in various studies or, eventually, a customized distance determined using a standing radiograph (Lerner et al., 2015).

In an earlier study, (Nissan, 1980) performed a sensitivity analysis by moving the CP 5 mm in the anterior-posterior direction and found that the posterior and anterior displacements would respectively increase the contact force by about 500N and decrease it by about 350N. More recently, Lerner et al. (2015) and Saliba et al. (2017) moved the CP locations only in the medial-lateral direction. They found that reducing the lever arm by moving the CP close to the knee joint fulcrum increased the contact forces in the corresponding compartment by a gradient up to 0.06 BW/mm. Therefore it is crucial to take into account the CP trajectories.

ACCEPTED MANUSCRIPT

Nevertheless, these authors computed the contact forces in a two-step procedure by considering the equilibrium of the contact forces, the musculo-tendon forces and the joint moment in the frontal plane. Therefore, they could not consider anterior-posterior shifting of the CP. Moreover, the modification of the CP trajectories was totally independent of the knee kinematics. In the light of articular surface geometrical complexity, recent experimental studies have demonstrated that each subject has a unique CP trajectory which showed medial-lateral and anterior-posterior excursions (Farrokhi et al., 2016; Li et al., 2015; Qi et al., 2013; Zeighami et al., 2017). The anterior-posterior and medial-lateral excursion of CPs in healthy subjects could reach 7.1 mm and 5.1 mm in 0º-30º flexion range (Zeighami et al., 2017). This excursion should be taken into account in contact force calculation.

To our knowledge, no study has yet estimated the contact forces along the subject-specific CP trajectories. The objective of the present study is to propose a new method to introduce subject-specific CP trajectories directly at the step of inverse kinematics, through relevant kinematic constraints. Moreover, similar to the anatomical constraints standing for the articular surfaces and ligaments (Moissenet et al., 2012, 2014), the Lagrange multipliers associated to these kinematic constraints stand straightforwardly for the contact forces at the medial and lateral CPs. This allows for a one-step procedure to compute simultaneously musculo-tendon forces and contact forces.

## Material and Methods

### *Musculoskeletal Model*



ACCEPTED MANUSCRIPT

ACCEPTED MANUSCRIPT

The musculoskeletal model of the lower limb used in the present study is the same as (Moissenet et al., 2014) except for the tibiofemoral joint constraints. The model is parameterized with natural coordinates $\mathbf{Q}_i$ where each segment is defined by two unitary directional vectors and two position vectors (De Jalon and Bayo, 2012; Dumas and Chèze, 2007). It consists of five segments, i.e. foot, shank, patella, thigh, and pelvis ($i$ = 1, …, 5). The hip joint is spherical and the patellofemoral and ankle joints are parallel mechanisms. Muscular lever arms were computed using the muscular geometry of Delp et al. (1990).

In the present study, the tibiofemoral joint ($T$) is modeled with five kinematics constraints:

$$\mathbf{\Phi}_T^k = \begin{pmatrix} \left(\mathbf{N}_4^{V_4^1}(\theta)\mathbf{Q}_4 - \mathbf{N}_2^{V_2^1}(\theta)\mathbf{Q}_2\right) \bullet \mathbf{N}_2^{\mathbf{X}_2}\mathbf{Q}_2 \\ \left(\mathbf{N}_4^{V_4^1}(\theta)\mathbf{Q}_4 - \mathbf{N}_2^{V_2^1}(\theta)\mathbf{Q}_2\right) \bullet \mathbf{N}_2^{\mathbf{Y}_2}\mathbf{Q}_2 \\ \left(\mathbf{N}_4^{V_4^1}(\theta)\mathbf{Q}_4 - \mathbf{N}_2^{V_2^1}(\theta)\mathbf{Q}_2\right) \bullet \mathbf{N}_2^{\mathbf{Z}_2}\mathbf{Q}_2 \\ \left(\mathbf{N}_4^{V_4^2}(\theta)\mathbf{Q}_4 - \mathbf{N}_2^{V_2^2}(\theta)\mathbf{Q}_2\right) \bullet \mathbf{N}_2^{\mathbf{X}_2}\mathbf{Q}_2 \\ \left(\mathbf{N}_4^{V_4^2}(\theta)\mathbf{Q}_4 - \mathbf{N}_2^{V_2^2}(\theta)\mathbf{Q}_2\right) \bullet \mathbf{N}_2^{\mathbf{Y}_2}\mathbf{Q}_2 \end{pmatrix} \quad \text{Eq. 1}$$

with $\mathbf{N}_i^{V_i^j}(\theta)$ the interpolation matrix for the $j^{\text{th}}$ virtual marker of the $i^{\text{th}}$ segment depending on the tibiofemoral extension-flexion angle $\theta$ and with $\mathbf{N}_2^{\mathbf{X}_2}$, $\mathbf{N}_2^{\mathbf{Y}_2}$, $\mathbf{N}_2^{\mathbf{Z}_2}$ the interpolation matrices for the axes of the tibia segment coordinate system. The interpolation matrices, $\mathbf{N}$, allow determining the position of any point (or the orientation of any direction) embedded in the relevant segment knowing its natural coordinates $\mathbf{Q}_i$.



ACCEPTED MANUSCRIPT

ACCEPTED MANUSCRIPT

Specifically, these virtual markers (i.e., $V_2^1$, $V_2^2$, $V_4^1$, and $V_4^2$) correspond to the medial and lateral CPs embedded in the shank and thigh segment, respectively. The position of these CPs is prescribed as a function of the tibiofemoral extension-flexion angle in the same way as the ligament lengths in (Gasparutto et al., 2015; Sancisi et al., 2017). The CP locations are provided in the supplementary material 1. Just like the coupling curves between the degrees of freedom introduced in many MSK models (Arnold et al., 2010; Delp et al., 1990; DeMers et al., 2014; Liu et al., 2008), there are five kinematic constraints at each position in extension-flexion of the joint. The medial CPs of tibia and femur were superimposed in the three directions of space while the lateral CPs of tibia and femur were superimposed only in the **X** (anterior-posterior) and **Y** (proximal-distal) directions of the shank.

The inverse kinematics step is formulated as:

$$\min_{\mathbf{Q}} f = \frac{1}{2}\left(\mathbf{\Phi}^m\right)^T \mathbf{\Phi}^m \quad \text{subject to} \quad \begin{pmatrix} \mathbf{\Phi}^k \\ \mathbf{\Phi}^r \end{pmatrix} = \mathbf{0} \quad , \qquad \text{Eq. 2}$$

with the complete definitions of the objective function *f*, driving constraints $\mathbf{\Phi}^m$, kinematic constraints $\mathbf{\Phi}^k$, and rigid body constraints $\mathbf{\Phi}^r$ detailed in (Duprey et al., 2010; El Habachi et al., 2015).

The kinematic constraints $\mathbf{\Phi}^k$ include all the constraints for ankle (*A*), patellofemoral (*P*), tibiofemoral (*T*) (i.e., $\mathbf{\Phi}_T^k$) and hip (*H*) joints.

The inverse dynamics step is then formulated as:



ACCEPTED MANUSCRIPT

ACCEPTED MANUSCRIPT

$$\begin{bmatrix}\mathbf{L} & -\mathbf{K}^T\end{bmatrix}\begin{pmatrix}\mathbf{f}\\ \boldsymbol{\lambda}\end{pmatrix} = \mathbf{G}\ddot{\mathbf{Q}} - \mathbf{R} - \mathbf{P}, \qquad \text{Eq. 3}$$

solved by the following optimization procedure:

$$\min_{\begin{pmatrix}\mathbf{f}\\ \boldsymbol{\lambda}_1\end{pmatrix}} J = \frac{1}{2}\begin{pmatrix}\mathbf{f}\\ \boldsymbol{\lambda}_1\end{pmatrix}^T \mathbf{W}\begin{pmatrix}\mathbf{f}\\ \boldsymbol{\lambda}_1\end{pmatrix}$$

$$\text{subject to } \begin{cases}\mathbf{Z}_{\mathbf{K}_2{}^T}\begin{bmatrix}\mathbf{L} & -\mathbf{K}_1{}^T\end{bmatrix}\begin{pmatrix}\mathbf{f}\\ \boldsymbol{\lambda}_1\end{pmatrix} = \mathbf{Z}_{\mathbf{K}_2{}^T}\left(\mathbf{G}\ddot{\mathbf{Q}} - \mathbf{P} - \mathbf{R}\right), \\ \begin{pmatrix}\mathbf{f}\\ \boldsymbol{\lambda}_1\end{pmatrix} \geq \mathbf{0}\end{cases} \qquad \text{Eq. 4}$$

with the complete definitions of the objective function *J*, the vector of musculo-tendon forces **f**, the Lagrange multipliers $\boldsymbol{\lambda}$, the sub-vector of Lagrange multipliers $\boldsymbol{\lambda}_1$ in the objective function, the optimisation weights matrix **W**, the projection matrix $\mathbf{Z}_{\mathbf{K}_2{}^T}$, the matrix of generalised muscular lever arms **L**, the Jacobian sub-matrix $\mathbf{K}_1$, the matrix of generalised masses **G**, the vector of generalised accelerations $\ddot{\mathbf{Q}}$, the vector of generalised weights **P**, and the vector of generalised ground reaction **R** detailed in Moissenet et al. (2014).

The two sub-matrices $\mathbf{K}_1$ and $\mathbf{K}_2$ of the Jacobian matrix $\mathbf{K} = \frac{\partial\begin{pmatrix}\boldsymbol{\Phi}^k\\ \boldsymbol{\Phi}^r\end{pmatrix}}{\partial\mathbf{Q}}$ are introduced to select the Lagrange multipliers to be included in the optimization and cancel the others with the projection matrix $\mathbf{Z}_{\mathbf{K}_2{}^T}$. As such, the Jacobian sub-matrix $\mathbf{K}_1$ includes,



ACCEPTED MANUSCRIPT

ACCEPTED MANUSCRIPT

among others, the derivatives $\frac{\partial \mathbf{\Phi}_T^k}{\partial \mathbf{Q}}$ and the corresponding Lagrange multipliers stand straightforwardly for the contact forces at the medial and lateral CPs and about the axes of the shank segment coordinate system.

The MSK modeling package runs on Matlab™. The simulation time of the MSK model for a single gait cycle was around 90 seconds.

*Experimental protocol*

Ten healthy (6 men, 4 women, 55.4 ± 9.5 yrs., 1.67 ± 0.10 m, 71.5 ± 13.3 kg) subjects walked with their comfortable speed on an instrumented split-belt treadmill (AMTI, Watertown, MA, USA) for 45 seconds. A 12-camera VICON system (Oxford Metrics, UK) recorded the 3D motion of the reflective markers mounted on the KneeKG™ (Emovi Inc., Laval, QC, Canada) system. Markers and force platform data were filtered using a 2nd order zero-lag Butterworth filter with automatic estimation of cut-off frequencies (Aissaoui et al., 2006). The joint angular displacements at the hip, knee, and ankle levels were assessed using a functional calibration method (Hagemeister et al., 2005). The joint kinematics and contact forces were normalized to 100% of the stance phase of gait. EMG signals of 8 muscles were collected to find the active/inactive concordance with the estimated Musculo-tendon forces (supplementary material 5). The experimental protocol was approved by the ethics committees of the Centre de recherche (CRCHUM) and the École de technologie supérieure de Montréal (ÉTS).

*CP trajectories*



ACCEPTED MANUSCRIPT

ACCEPTED MANUSCRIPT

Three CP trajectory models were used in the MSK model. The corresponding polynomial equations are presented in the Supplementary material 1.

1) Linear CP trajectory (LCP): This model represents the general assumptions made in many MSK models (Johnson et al., 1981; Lerner et al., 2015; Lloyd and Buchanan, 1996; Morrison, 1970; Saliba et al., 2017; Winby et al., 2009). The contact forces, musculo-tendon forces and joint moment are only balanced in the frontal plane of the tibia at a given distance from the tibial plateau centreline. To build the complying version of the model to the Eq. 1, the tibial CPs were represented by two straight lines in the sagittal plane as in Lemieux et al. (2016). The medial-lateral CP locations were fixed at 20 mm from the centreline and the anterior-posterior location of the CPs was driven by a regression equation as a function of flexion angle (Delp et al., 1990; Nisell et al., 1986).

2) Sphere-on-plane trajectory (SPP): The CP trajectories represent the femur/tibia sphere-on-plane contact mechanism guided by three isometric ligaments. (Duprey et al., 2010; Feikes et al., 2003). The mechanism geometry is based on *in vitro* measurements (Parenti-Castelli and Sancisi, 2013), and was not personalized.

3) Personalized CP trajectory (PCP): The CP trajectories were interpolated from the weighted center of bone-to-bone proximity measured during a quasi-static squatting task. Bi-plane X-ray images of the lower limb were recorded at $0^{o}$, $15^{o}$, $30^{o}$, $45^{o}$, and $70^{o}$ of knee flexion using the EOS$^{TM}$ low-dose imaging system (EOS Imaging, Paris, France). The accuracy of estimating the weighted center of bone-to-bone proximity was reported 2 mm in the anterior-posterior and 3 mm in the medial-lateral directions in a simulation test (Zeighami et al., 2017).



ACCEPTED MANUSCRIPT

ACCEPTED MANUSCRIPT

Once the CP trajectories are found in thigh and shank segment coordinate system (as a function of $\theta$), the terms of Eq. 1 are obtained (see Supplementary material 2) using the matrix **B** relating the natural coordinates $\mathbf{Q}_i$ with the segment axes (Dumas and Chèze, 2007).

*Statistical Analysis:*

One-way repeated measures analysis of variance (ANOVA) was performed to detect statistically significant differences in contact forces estimated using the three CP trajectory methods ($p<0.05$). Bonferroni post-hoc test detected the pair-wise differences. In the PCP model, a linear correlation test was performed to find the possible correlation between the medial peak forces and the anterior-posterior and medial-lateral locations of the medial CPs, and between the lateral peak forces and the anterior-posterior and medial-lateral locations of the lateral CPs.

**Results**

The trajectories of PCP and SPP models showed a distinct deviation from the LCP model on the medial and lateral compartments both in medial-lateral and anterior-posterior directions as shown for a sample subject in Figure (1). The CP trajectories had a remarkable impact on the knee joint kinematics as well as the contact forces (Figure 2). However, this impact varied widely among the subjects.



ACCEPTED MANUSCRIPT

ACCEPTED MANUSCRIPT

For instance, the first peak of the medial contact forces estimated from the PCP model with respect to the LCP model, increased from 1.43 BW to 2.46 BW in subject N4, whereas it decreased from 1.45 BW to 1.32 BW in subject N2 (Table 1).

The maximum difference in estimating the first medial peak between the PCP and LCP models was 1.03 BW in subject N4, between the PCP and SPP models was 0.65 BW in subject N5, and between the LCP and SPP models was 0.89 BW in subject N1. The maximum difference in estimating the first lateral peak between the PCP and LCP models was 0.64 BW in subject N5, between the PCP and SPP models was 0.25 BW in subject N5, and between the LCP and SPP models was 0.50 BW in subject N8 (Table 1).

The average second peak of the medial contact force was significantly higher in the SPP model (2.88 BW) compared to the LCP (2.07 BW) and PCP (1.87 BW) models ($p<0.05$). The second peak of the total contact force was also greater in the SPP model, however, the difference was not significant ($p=0.10$). In general, the LCP and PCP models demonstrated closer estimations compared to the SPP model (Figure 3).

All the medial compartment CPs in the PCP model were located lateral to the LCP model CPs. The first peak medial contact forces in PCP increased in six subjects and slightly decreased in four subjects with respect to the LCP model (Supplementary material 3) (Table 1). Similarly, on the lateral side, the direction of the CP shift could not predict the direction of the change in the lateral contact forces with respect to the LCP model.

The PCP model generally suggested lower medial contact forces when the CPs were more medially located (Figure 4). A moderate positive correlation existed between the peaks of medial contact forces and the medial-lateral location of the medial CPs ($r=0.53$,



ACCEPTED MANUSCRIPT

ACCEPTED MANUSCRIPT

p<0.001). Conversely, no correlation was observed in the lateral compartment (Figure 4). No correlation was found between the peaks of medial (r=0.14, p=0.54) and lateral (r=0.1, p=0.6) contact forces and anterior-posterior location of the CPs.

**Discussion**

The present study focuses on inverse dynamics computational frameworks where the personalization of the joints relies on the kinematic constraints and/or model geometrical parameters. In the literature, the joint kinematics and the position of the CPs appear to be treated independently (Gerus et al., 2013; Lerner et al., 2015; Saliba et al., 2017). In our formulation, it appears clearly that the subject-specific kinematics constraints $\mathbf{\Phi}_T^k$ and contact forces (i.e., the Lagrange multipliers associated to $\frac{\partial \mathbf{\Phi}_T^k}{\partial \mathbf{Q}}$) are directly related. Therefore, the joint kinematics were correspondingly adapted to the subject-specific CP trajectories and contributed to the contact force. Certain knee joint constraints such as sphere-on-plane mechanism could be personalized based on the anatomical measures from bi-plane radiography (Clément et al., 2015, 2017) or MRI (da Luz et al., 2017). However, the kinematics constraints proposed in Eq. 1 are certainly the most versatile ones as they can be deduced from any joint model and geometry. As such, they have been used in the present study to compare two tibiofemoral joints of the literature (Delp et al., 1990; Moissenet et al., 2014) as well as to integrate personalized CP measurements obtained by quasi-static squat (Zeighami et al., 2016). Future works could integrate the personalized CP trajectories obtained from methods such as bi-plane fluoroscopy within the same activity i.e., treadmill walking.



ACCEPTED MANUSCRIPT

ACCEPTED MANUSCRIPT

Within the simulated finite element computational frameworks, subject-specific joint models can also be built including detailed deformable geometry. The CP trajectories are therefore not inputs but rather outputs of the model together with the contact forces (Lenhart et al., 2015b; Marouane et al., 2016). It allows these models to simulate relationships between joint structure and mechanics. Nevertheless, the computed CPs could vary from the experimentally measured CPs since several parameters including the stiffness of the ligament with a high impact on the CPs (Lenhart et al., 2015a) cannot be personalized. To our knowledge, the present study is the first to implement the experimentally measured CP trajectories into the inverse kinematics and contact force calculation steps.

Our study showed that using the PCP model in certain subjects increased the estimated peak contact forces up to 1.03 BW (subject N4) and 0.65 BW (subject N5) on the medial and lateral sides compared to the LCP model (Table 1). For these two specific subjects, a remarkable increase in the vastus medialis and vastus lateralis muscle forces were observed in the PCP model, which is not the case in the other subjects (Supplementary material 4). According to the Lerner et al. (2015) gradient, the medial contact force in subject N4 would have increased by 0.44 BW due to 7.4 mm lateral shift of the CP, and the lateral contact force in subject N4 would have decreased by 0.64 BW due to the 10.7 mm lateral shift of the CP. The estimated contact forces could vary largely when different CP trajectory models were used. However, the difference between the average contact forces from the three models was significant only in the second peak of medial contact force (Figure 3). The contact force variations were generally larger on the medial side. The sphere-on-plane model tended to show larger differences with respect to the other two models (Figure 3).

Our results showed that the medial-lateral shift of the CPs alone could not determine the increase/decrease pattern of the contact forces. Lerner et al. (2015) and Saliba et al. (2017) reported that if the CPs were shifted medially the medial contact force would



ACCEPTED MANUSCRIPT

ACCEPTED MANUSCRIPT

decrease and the lateral contact force would increase by 1-6% BW/mm. Our results showed that there is no correlation for the lateral contact, yet a moderate relationship existed for the medial contact (Figure 4). Lack of a strong relationship between the contact location shifts and the medial/lateral force was not unexpected in our multifactorial study. In Lerner et al. (2015) and Saliba et al. (2017), the musculotendon forces are first calculated and the joint equilibrium in the frontal plane determines the contact forces. In this study, the musculotendon forces and the contact forces were calculated in one step and the equilibrium was attained in all planes. In addition, the kinematics of the joints was affected by the alteration of the CP trajectories. It has been long known that the contact locations are non-straight subject-specific paths (Ahmed and Burke, 1983) and that the CP locations alter the contact force estimation (Nissan, 1980). Therefore, the change in the CP distance from the tibial plateau centreline was not adequate in estimating the medial/lateral contact force.

Moreover, the CP trajectories are significantly altered in knee pathologies such as osteoarthritis (Farrokhi et al., 2016; Li et al., 2015; Zeighami et al., 2017); yet still most of the MSK models use the LCP-like models to estimate the medial/lateral contact forces both for osteoarthritic subjects and healthy controls (Kumar et al., 2013). Our method may serve to further personalize tibiofemoral joints in the MSK models and to develop a more realistic estimation of contact forces in osteoarthritic population.

The MSK model used in this study was previously validated using knee instrumented implant data (Moissenet et al., 2014, 2016; Moissenet et al., 2015). With the SPP model, it could predict the medial and lateral contact forces with a mean RMSE difference of 0.39 BW and 0.28 BW (Moissenet et al., 2014). Unfortunately, there is no means to validate the PCP model. To check if the results were realistic or not a pseudo-validation using EMG data was used (Supplementary material 5). EMG results revealed no remarkable



ACCEPTED MANUSCRIPT

ACCEPTED MANUSCRIPT

difference between the three CP trajectory models yet, the PCP model demonstrated a slightly better concordance with EMG data for rectus femoris and vasti muscle that are two main contributors to the first peak contact force (Moissenet et al., 2017).

The main limitation of this study is the application of CP trajectories extracted from a quasi-static squat into the gait. Indeed, a mismatch between the kinematics of the tibiofemoral joint would result in different CP trajectories. Nevertheless, Gasparutto et al. (2017) synthesized the kinematics of the normal knee during various weight-bearing activities measured by intra-cortical pins and bi-plane fluoroscopy and concluded that the impact of the dynamic activity on the couplings between the joint degrees of freedom was limited. Treadmill walking also creates some differences in the kinematics of the gait (Alton et al., 1998; Murray et al., 1964; Strathy et al., 1983; Warabi et al., 2005). However, this latter applies to all the 3 models used in this study and is not likely to affect the conclusion regarding the difference between the models. The other limitation of this work is the accuracy of the measured CPs. The accuracy of the bone-to-bone proximity estimation was reported <3mm (Zeighami et al., 2017). The CPs at the five flexion angles were interpolated to find the trajectory as a function of knee extension-flexion that may add further errors. Moreover, cartilage thickness is not uniformly distributed over the joint regions (Favre et al., 2017). Therefore our method relying solely on bone proximity and neglecting cartilage thickness could be biased to predict CPs in regions with minimal cartilage (DeFrate et al., 2004; Marouane et al., 2016). Finally, the definition of the CP has to be clarified. Since there is no practical way to measure the center of pressure in the menisci and cartilage, a weighted center of bone-to-bone proximity was considered as the CP location.

This study introduced a new method to incorporate personalized CP trajectories in the MSK model contact force estimations. Currently, the CP trajectories are based on biplane radiography during squat which is subjected to limitations. But, more precise



ACCEPTED MANUSCRIPT

ACCEPTED MANUSCRIPT

dynamic CP trajectories by considering layers of cartilage and menisci tissues could be introduced the same way in the proposed model. The impact of changing the CP trajectories on the medial/lateral contact forces was substantially large and was variable between the medial/lateral compartments and among the subjects. Due to the multifactorial nature of contact force calculations, the medial-lateral shift of the CP distance from the tibial plateau centreline alone could not predict the direction of compartmental contact force changes.

**Conflicts of interest**

There are no conflicts of interest to report.

**Acknowledgements**

The present work was supported by the Fonds de Recherche du Québec en Santé (FRQ-S), the Fonds de Recheche du Québec en Nature et Technologie (FRQ-NT) and the Natural Science and Research Council of Canada (NSERC). This work was performed within the framework of the LABEX PRIMES (ANR-11-LABX-0063) of Université de Lyon, within the program "Investissements d'Avenir" (ANR-11-IDEX-0007) operated by the French National Research Agency (ANR).



ACCEPTED MANUSCRIPT

ACCEPTED MANUSCRIPT

## References

Ahmed, A., Burke, D., 1983. In-vitro of measurement of static pressure distribution in synovial joints—Part I: Tibial surface of the knee. Journal of biomechanical engineering 105, 216-225.

Aissaoui, R., Husse, S., Mecheri, H., Parent, G., De Guise, J., Year Automatic filtering techniques for three-dimensional kinematics data using 3D motion capture system. In Industrial Electronics, 2006 IEEE International Symposium on.

Alton, F., Baldey, L., Caplan, S., Morrissey, M., 1998. A kinematic comparison of overground and treadmill walking. Clinical biomechanics 13, 434-440.

Arnold, E.M., Ward, S.R., Lieber, R.L., Delp, S.L., 2010. A Model of the Lower Limb for Analysis of Human Movement. Annals of biomedical engineering 38, 269-279.

Clément, J., Dumas, R., Hagemeister, N., De Guise, J.A., 2015. Soft tissue artifact compensation in knee kinematics by multi-body optimization: performance of subject-specific knee joint models. Journal of Biomechanics 48, 3796-3802.

Clément, J., Dumas, R., Hagemeister, N., De Guise, J.A., 2017. Can generic knee joint models improve the measurement of osteoarthritic knee kinematics during squatting activity? Computer methods in biomechanics and biomedical engineering 20, 94-103.

Crowninshield, R.D., 1978. Use of Optimization Techniques to Predict Muscle Forces. Journal of biomechanical engineering 100, 88-92.

da Luz, S.B., Modenese, L., Sancisi, N., Mills, P.M., Kennedy, B., Beck, B.R., Lloyd, D.G., 2017. Feasibility of using MRIs to create subject-specific parallel-mechanism joint models. Journal of Biomechanics 53, 45-55.

De Jalon, J.G., Bayo, E., 2012. Kinematic and dynamic simulation of multibody systems: the real-time challenge. Springer Science & Business Media.

DeFrate, L.E., Sun, H., Gill, T.J., Rubash, H.E., Li, G., 2004. In vivo tibiofemoral contact analysis using 3D MRI-based knee models. Journal of Biomechanics 37, 1499-1504.

Delp, S.L., Loan, J.P., Hoy, M.G., Zajac, F.E., Topp, E.L., Rosen, J.M., 1990. An interactive graphics-based model of the lower extremity to study orthopaedic surgical procedures. IEEE Transactions on Biomedical engineering 37, 757-767.

DeMers, M.S., Pal, S., Delp, S.L., 2014. Changes in tibiofemoral forces due to variations in muscle activity during walking. Journal of Orthopaedic Research 32, 769-776.

Draganich, L., Andriacchi, T., Andersson, G., 1987. Interaction between intrinsic knee mechanics and the knee extensor mechanism. Journal of Orthopaedic Research 5, 539-547.

Dumas, R., Chèze, L., 2007. 3D inverse dynamics in non-orthonormal segment coordinate system. Medical & Biological Engineering & Computing 45, 315-322.

Duprey, S., Cheze, L., Dumas, R., 2010. Influence of joint constraints on lower limb kinematics estimation from skin markers using global optimization. Journal of Biomechanics 43, 2858-2862.



ACCEPTED MANUSCRIPT

ACCEPTED MANUSCRIPT

El Habachi, A., Duprey, S., Cheze, L., Dumas, R., 2015. A parallel mechanism of the shoulder—application to multi-body optimisation. Multibody System Dynamics 33, 439-451.

Farrokhi, S., Voycheck, C.A., Gustafson, J.A., Fitzgerald, G.K., Tashman, S., 2016. Knee joint contact mechanics during downhill gait and its relationship with varus/valgus motion and muscle strength in patients with knee osteoarthritis. The Knee 23, 49-56.

Farrokhi, S., Voycheck, C.A., Klatt, B.A., Gustafson, J.A., Tashman, S., Fitzgerald, G.K., 2014. Altered tibiofemoral joint contact mechanics and kinematics in patients with knee osteoarthritis and episodic complaints of joint instability. Clinical biomechanics 29, 629-635.

Favre, J., Erhart-Hledik, J.C., Blazek, K., Fasel, B., Gold, G.E., Andriacchi, T.P., 2017. Anatomically Standardized Maps Reveal Distinct Patterns of Cartilage Thickness With Increasing Severity of Medial Compartment Knee Osteoarthritis. Journal of Orthopaedic Research.

Feikes, J., O'Connor, J., Zavatsky, A., 2003. A constraint-based approach to modelling the mobility of the human knee joint. Journal of Biomechanics 36, 125-129.

Gasparutto, X., Moissenet, F., Lafon, Y., Chèze, L., Dumas, R., 2017. Kinematics of the Normal Knee during Dynamic Activities: A Synthesis of Data from Intracortical Pins and Biplane Imaging. Applied Bionics and Biomechanics 2017.

Gasparutto, X., Sancisi, N., Jacquelin, E., Parenti-Castelli, V., Dumas, R., 2015. Validation of a multi-body optimization with knee kinematic models including ligament constraints. Journal of Biomechanics 48, 1141-1146.

Gerus, P., Sartori, M., Besier, T.F., Fregly, B.J., Delp, S.L., Banks, S.A., Pandy, M.G., D'Lima, D.D., Lloyd, D.G., 2013. Subject-specific knee joint geometry improves predictions of medial tibiofemoral contact forces. Journal of Biomechanics 46, 2778-2786.

Hagemeister, N., Parent, G., Van de Putte, M., St-Onge, N., Duval, N., de Guise, J., 2005. A reproducible method for studying three-dimensional knee kinematics. Journal of Biomechanics 38, 1926-1931.

Johnson, F., Scarrow, P., Waugh, W., 1981. Assessments of loads in the knee joint. Medical and Biological Engineering and Computing 19, 237-243.

Jung, Y., Phan, C.-B., Koo, S., 2016. Intra-Articular Knee Contact Force Estimation During Walking Using Force-Reaction Elements and Subject-Specific Joint Model. Journal of biomechanical engineering 138, 021016.

Kia, M., Stylianou, A.P., Guess, T.M., 2014. Evaluation of a musculoskeletal model with prosthetic knee through six experimental gait trials. Medical Engineering & Physics 36, 335-344.

Kumar, D., Manal, K.T., Rudolph, K.S., 2013. Knee joint loading during gait in healthy controls and individuals with knee osteoarthritis. Osteoarthritis and Cartilage 21, 298-305.

Lemieux, P.-O., Cresson, T., Aissaoui, R., 2016. Simultaneous estimation of the path, magnitude and orientation of the femorotibial contact forces using bone geometry constraints: an exploratory numerical study for the stance phase of gait. Multibody System Dynamics, 1-21.

Lenhart, R.L., Kaiser, J., Smith, C.R., Thelen, D.G., 2015a. Prediction and validation of load-dependent behavior of the tibiofemoral and patellofemoral joints during movement. Annals of biomedical engineering 43, 2675-2685.

Lenhart, R.L., Smith, C.R., Vignos, M.F., Kaiser, J., Heiderscheit, B.C., Thelen, D.G., 2015b. Influence of step rate and quadriceps load distribution on patellofemoral cartilage contact pressures during running. Journal of Biomechanics 48, 2871-2878.

Lerner, Z.F., DeMers, M.S., Delp, S.L., Browning, R.C., 2015. How tibiofemoral alignment and contact locations affect predictions of medial and lateral tibiofemoral contact forces. Journal of Biomechanics 48, 644-650.



ACCEPTED MANUSCRIPT

ACCEPTED MANUSCRIPT

Li, C., Hosseini, A., Tsai, T.Y., Kwon, Y.M., Li, G., 2015. Articular contact kinematics of the knee before and after a cruciate retaining total knee arthroplasty. Journal of Orthopaedic Research 33, 349-358.
Liu, M.Q., Anderson, F.C., Schwartz, M.H., Delp, S.L., 2008. Muscle contributions to support and progression over a range of walking speeds. Journal of Biomechanics 41, 3243-3252.
Lloyd, D., Buchanan, T., 1996. A model of load sharing between muscles and soft tissues at the human knee during static tasks. TRANSACTIONS-AMERICAN SOCIETY OF MECHANICAL ENGINEERS JOURNAL OF BIOMECHANICAL ENGINEERING 118, 367-376.
Marouane, H., Shirazi-Adl, A., Adouni, M., 2016. Alterations in knee contact forces and centers in stance phase of gait: a detailed lower extremity musculoskeletal model. Journal of Biomechanics 49, 185-192.
Marra, M.A., Vanheule, V., Fluit, R., Koopman, B.H.F.J.M., Rasmussen, J., Verdonschot, N., Andersen, M.S., 2015. A Subject-Specific Musculoskeletal Modeling Framework to Predict In Vivo Mechanics of Total Knee Arthroplasty. Journal of biomechanical engineering 137, 020904-020904-020912.
Moissenet, F., Cheze, L., Dumas, R., 2017. Individual muscle contributions to ground reaction and to joint contact, ligament and bone forces during normal gait. Multibody System Dynamics 40, 193-211.
Moissenet, F., Chèze, L., Dumas, R., 2012. Anatomical kinematic constraints: consequences on musculo-tendon forces and joint reactions. Multibody System Dynamics 28, 125-141.
Moissenet, F., Chèze, L., Dumas, R., 2014. A 3D lower limb musculoskeletal model for simultaneous estimation of musculo-tendon, joint contact, ligament and bone forces during gait. Journal of Biomechanics 47, 50-58.
Moissenet, F., Chèze, L., Dumas, R., 2016. Influence of the level of muscular redundancy on the validity of a musculoskeletal model. Journal of biomechanical engineering 138, 021019.
Moissenet, F., Giroux, M., Chèze, L., Dumas, R., 2015. Validity of a musculoskeletal model using two different geometries for estimating hip contact forces during normal walking. Computer methods in biomechanics and biomedical engineering 18, 2000-2001.
Morrison, J., 1970. The mechanics of the knee joint in relation to normal walking. Journal of Biomechanics 3, 51-61.
Murray, M.P., Drought, A.B., Kory, R.C., 1964. Walking patterns of normal men. JBJS 46, 335-360.
Nisell, R., Németh, G., Ohlsén, H., 1986. Joint forces in extension of the knee: analysis of a mechanical model. Acta Orthopaedica Scandinavica 57, 41-46.
Nissan, M., 1980. Review of some basic assumptions in knee biomechanics. Journal of Biomechanics 13, 375-381.
Parenti-Castelli, V., Sancisi, N., 2013. Synthesis of spatial mechanisms to model human joints, 21st century kinematics. Springer, pp. 49-84.
Qi, W., Hosseini, A., Tsai, T.-Y., Li, J.-S., Rubash, H.E., Li, G., 2013. In vivo kinematics of the knee during weight bearing high flexion. Journal of Biomechanics 46, 1576-1582.
Saliba, C.M., Brandon, S.C., Deluzio, K.J., 2017. Sensitivity of medial and lateral knee contact force predictions to frontal plane alignment and contact locations. Journal of Biomechanics.
Sancisi, N., Gasparutto, X., Parenti-Castelli, V., Dumas, R., 2017. A multi-body optimization framework with a knee kinematic model including articular contacts and ligaments. Meccanica 52, 695-711.



ACCEPTED MANUSCRIPT

ACCEPTED MANUSCRIPT

Scheys, L., Desloovere, K., Spaepen, A., Suetens, P., Jonkers, I., 2011. Calculating gait kinematics using MR-based kinematic models. Gait & posture 33, 158-164.
Schipplein, O., Andriacchi, T., 1991. Interaction between active and passive knee stabilizers during level walking. Journal of Orthopaedic Research 9, 113-119.
Strathy, G., Chao, E., Laughman, R., 1983. Changes in knee function associated with treadmill ambulation. Journal of Biomechanics 16, 517521-519522.
Valente, G., Pitto, L., Stagni, R., Taddei, F., 2015. Effect of lower-limb joint models on subject-specific musculoskeletal models and simulations of daily motor activities. Journal of Biomechanics 48, 4198-4205.
Warabi, T., Kato, M., Kiriyama, K., Yoshida, T., Kobayashi, N., 2005. Treadmill walking and overground walking of human subjects compared by recording sole-floor reaction force. Neuroscience research 53, 343-348.
Winby, C.R., Lloyd, D.G., Besier, T.F., Kirk, T.B., 2009. Muscle and external load contribution to knee joint contact loads during normal gait. Journal of Biomechanics 42, 2294-2300.
Zeighami, A., Dumas, R., Aissaoui, R., 2016. Medial and lateral knee joint contact forces during gait in normal and osteoarthritic subjects. In Virtual Physiological Human Conference VPH2016.
Zeighami, A., Dumas, R., Kanhonou, M., Hagemeister, N., Lavoie, F., De Guise, J., Aissaoui, R., 2017. Tibio-femoral joint contact in healthy and osteoarthritic knees during quasi-static squat: A bi-planar X-ray analysis. Journal of Biomechanics 53, 178-184.
Zheng, L., Li, K., Shetye, S., Zhang, X., 2014. Integrating dynamic stereo-radiography and surface-based motion data for subject-specific musculoskeletal dynamic modeling. Journal of Biomechanics 47, 3217-3221.



ACCEPTED MANUSCRIPT

ACCEPTED MANUSCRIPT

Figure 1 CP trajectories of subject N10 from the three CP trajectory models over the tibial plateau: linear CP (LCP) trajectory (: black), sphere-on-plane (SPP) trajectory (-- blue), and personalized CP (PCP) trajectory (- red) models. The sequence of stance phase events is illustrated on each CP trajectory: first and second peaks of medial (pk1 Med, pk2 Med), first and second peaks of lateral (pk1 Lat, pk2 Lat) contact force, heel strike (HS), toe off (TO), $0^{o}$ (flx0) and $70^{o}$ (flx70) knee flexion. The shaded region around the PCP model represents uncertainty of estimating the weighted center of bone-to-bone proximity (±3 mm) in the medial-lateral direction (Zeighami et al. 2016).

Figure 2 Medial, lateral, and total contact forces as well as the knee extension-flexion (Ext-Flex), adduction- abduction (Add-Abd), Internal-external (Int-Ext) rotations, lateral-medial (Lat-Med), anterior-posterior (Ant-Post), and proximal-distal (Prox-Dist) translations of subject N10 using the linear CP (LCP) trajectory (:black), sphere-on-plane (SPP) trajectory (--blue), and personalized CP (PCP) trajectory (-red) models. The corresponding CP trajectories are presented in Figure (1).

Figure 3 The average (10 subjects) first and second peaks of medial (pk1 Med, pk2 Med) , first and second peaks of lateral (pk1 Lat, pk2 Lat) , first and second peaks of total (pk1 T, pk2 T) contact forces using the linear CP (LCP) trajectory, sphere-on-plane (SPP) trajectory, and personalized CP (PCP) trajectory models. * and @ denote statistically significant differences between the SPP and LCP models and between the SPP and PCP models, respectively.



ACCEPTED MANUSCRIPT

ACCEPTED MANUSCRIPT

Figure 4 First (red markers) and second (blue markers) peaks of the medial and lateral contact forces (pk1 Med, pk2 Med, pk1 Lat, pk2 Lat) from the personalized CP trajectory (PCP) model and the location of the personalized CPs at the corresponding events. Coordinates of the points are presented in Table 1 for all 10 subjects. Dashed line represents the regression line on the medial side ($r=0.53$, $p<0.001$). No correlation existed on the lateral side ($r=0.18$, $p=0.43$). Results adapted from two previous sensitivity analysis studies are also presented. The range of CP perturbations were ±10 mm (from a ±25 mm position of the CPs with respect to centerline) in Saliba et al. (2017), and ±4 mm (from a ±20 mm position of the CPs with respect to centerline) in Lerner et al. (2016).



ACCEPTED MANUSCRIPT

ACCEPTED MANUSCRIPT

Table 1 (a) characteristics of the ten subjects in this study. (b) First and second peaks of the medial and lateral (pk1Med, pk2Med, pk1Lat, pk2Lat) contact forces from the linear CP trajectory (LCP) , sphere-on-plane (SPP) trajectory, and personalized CP (PCP) trajectory models, and location of the CPs in medial (M) – lateral (L) and anterior (A) – posterior (P) directions of the tibial plateau at the corresponding events.

| | | | | | (b) | | | | | | | | | | | | | | | | | |
|---|---|---|---|---|---|---|---|---|---|---|---|---|---|---|---|---|---|---|---|---|---|---|
| | (a) | | | | LCP(pk1 Med) | | | LCP(pk1Lat) | | | SPP(pk1Med) | | | SPP(pk1Lat) | | | PCP(pk1Med) | | | PCP(pk1Lat) | | |
| subject | subject characteristics | | | | Medial Contact force (BW) | Medial CP (mm) | | Lateral contact force (BW) | Lateral CP (mm) | | Medial Contact force (BW) | Medial CP (mm) | | Lateral contact force (BW) | Lateral CP (mm) | | Medial Contact force (BW) | Medial CP (mm) | | Lateral contact force (BW) | Lateral CP (mm) | |
| | Gendre | Age (yrs) | Weight(kg) | Height(m) | | M(+) - L(-) | A(+) - P(-) | | M(+) - L(-) | A(+) - P(-) | | M(+)- L(-) | A(+) - P(-) | | M(+) - L(-) | A(+) - P(-) | | M(+) - L(-) | A(+) - P(-) | | M(+) - L(-) | A(+) - P(-) |
| N1 | M | 39 | 76.9 | 1.73 | 1.9 | -20 | 2.64 | 1.43 | 20 | 1.80 | 2.79 | -23.3 | -4.92 | 1.81 | 22.2 | -5.89 | 2.32 | -8.9 | 9.41 | 1.09 | 13.5 | 2.22 |
| N2 | M | 66 | 54 | 1.5 | 1.45 | -20 | 0.90 | 0.92 | 20 | -0.85 | 1.36 | -23.8 | -5.79 | 1.32 | 21.5 | -8.85 | 1.32 | -14.4 | 1.86 | 0.97 | 18.9 | -11.62 |
| N3 | M | 38 | 84.5 | 1.71 | 1.18 | -20 | 2.30 | 1.34 | 20 | 1.14 | 1.36 | -23.4 | -5.07 | 1.81 | 22.1 | -6.42 | 1.15 | -10.4 | 13.33 | 1.8 | 16.8 | 5.26 |
| N4 | F | 57 | 58.1 | 1.66 | 1.43 | -20 | 2.27 | 1.67 | 20 | 0.88 | 2.09 | -23.2 | -4.78 | 1.79 | 22.2 | -6.25 | 2.46 | -12.6 | 9.97 | 1.6 | 22.5 | 0.90 |
| N5 | M | 61 | 81.9 | 1.81 | 1.3 | -20 | 1.77 | 0.76 | 20 | 1.74 | 1.45 | -23.5 | -5.13 | 1.15 | 22.3 | -5.70 | 2.1 | -12.7 | 13.66 | 1.4 | 30.6 | -0.52 |
| N6 | F | 60 | 60.8 | 1.64 | 1.01 | -20 | 1.36 | 1.86 | 20 | 0.94 | 1.44 | -23.4 | -5.09 | 2.32 | 22 | -6.82 | 0.99 | -17.9 | 6.36 | 2.14 | 18.5 | -3.00 |
| N7 | M | 61 | 89.8 | 1.73 | 1.69 | -20 | 5.61 | 0.26 | 20 | 5.61 | 2.08 | -22.8 | -4.42 | 0.27 | 22.7 | -0.91 | 1.78 | -15.2 | 13.17 | 0.22 | 17.5 | 4.30 |
| N8 | F | 60 | 58.3 | 1.56 | 1.49 | -20 | 4.47 | 0.99 | 20 | 3.19 | 1.51 | -23 | -4.56 | 1.49 | 22.4 | -4.58 | 1.45 | -12.6 | 10.65 | 1.2 | 20.8 | 4.36 |



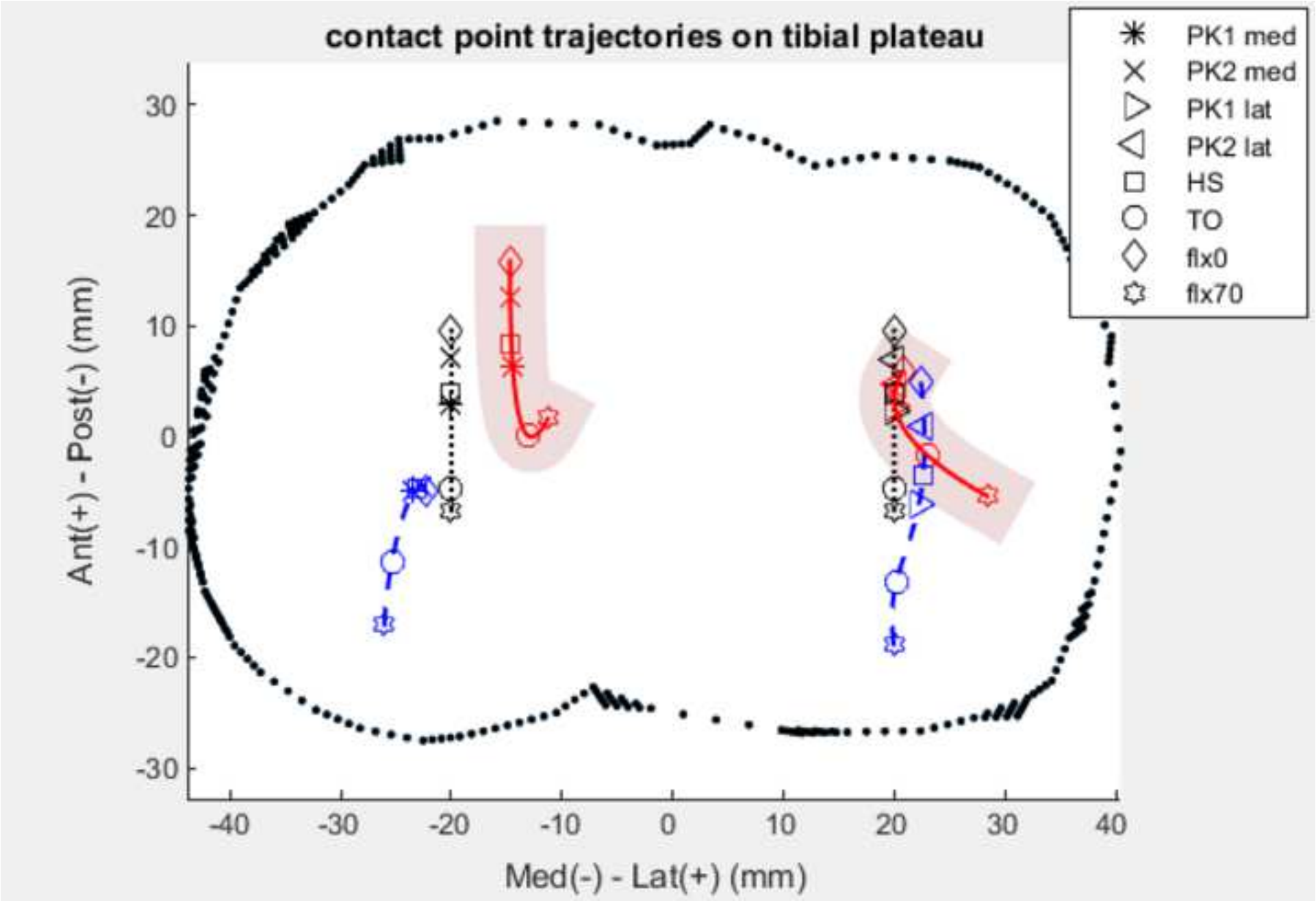
ACCEPTED MANUSCRIPT

ACCEPTED MANUSCRIPT

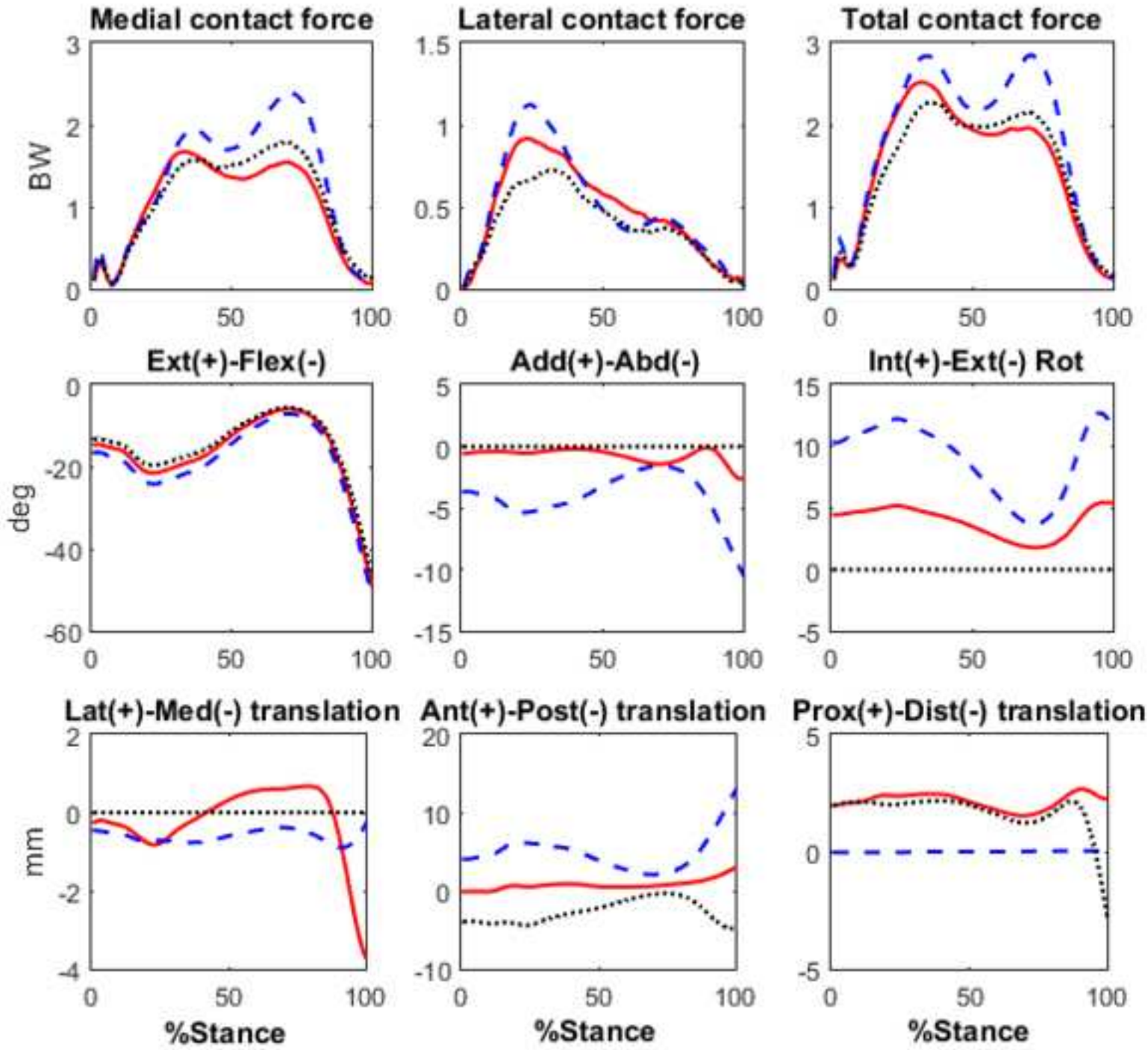
| | | | | | | | | | | | | | | | | | | | | | |
|---|---|---|---|---|---|---|---|---|---|---|---|---|---|---|---|---|---|---|---|---|---|
| N9 | M | 59 | 80.7 | 1.75 | 0.71 | -20 | 4.81 | 1.1 | 20 | 3.55 | 0.66 | -23 | -4.53 | 1.37 | 22.5 | -3.67 | 1.02 | -15.2 | 12.57 | 0.88 | 24.8 | -0.23 |
| N10 | F | 53 | 60.6 | 1.59 | 1.59 | -20 | 2.88 | 0.72 | 20 | 2.33 | 1.94 | -23.4 | -5.00 | 1.12 | 22.2 | -6.17 | 1.67 | -14.4 | 6.40 | 0.92 | 20 | 2.64 |

ACCEPTED MANUSCRIPT

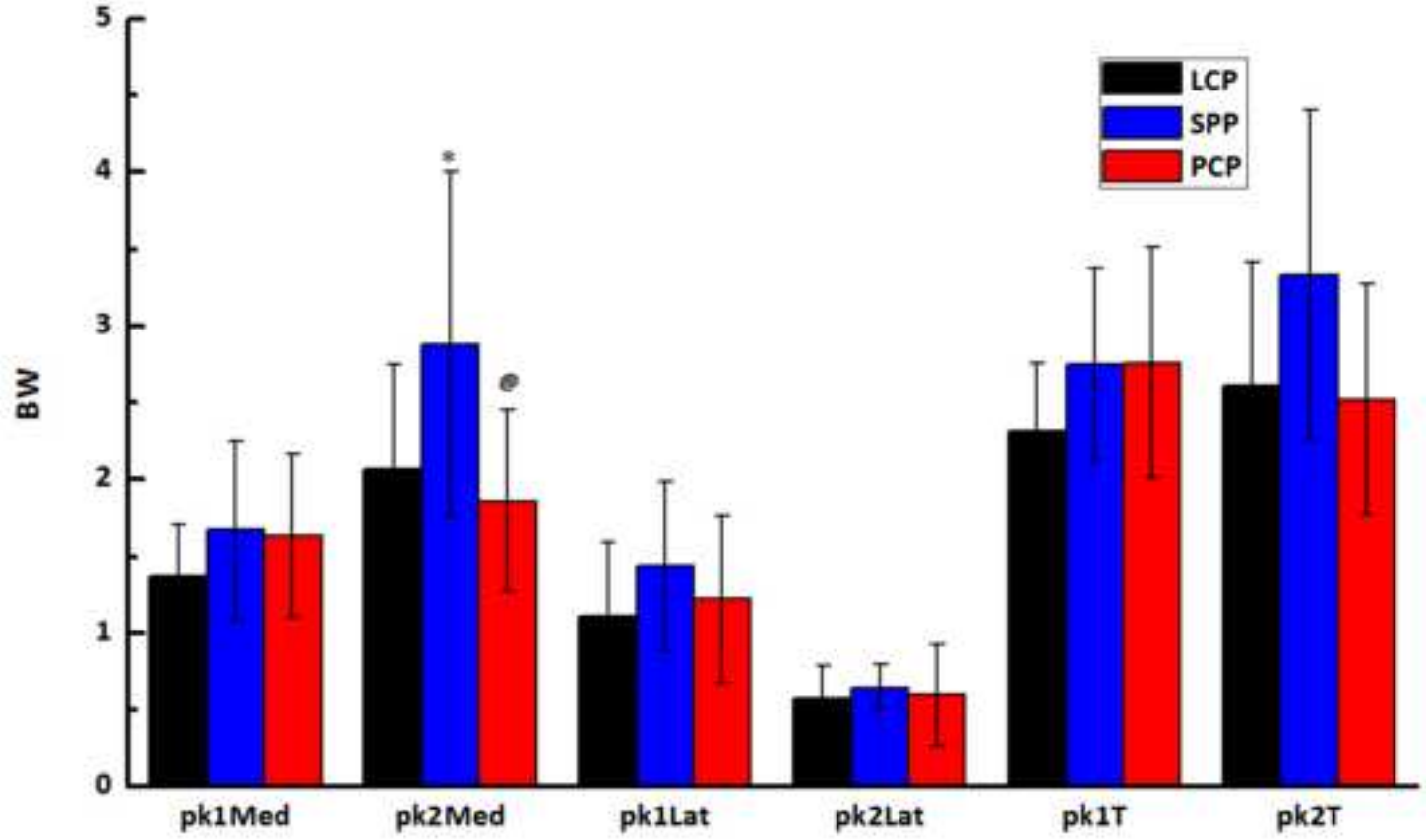
ACCEPTED MANUSCRIPT



ACCEPTED MANUSCRIPT



ACCEPTED MANUSCRIPT



ACCEPTED MANUSCRIPT

